DESIGN OF ULTRA-HIGH TEMPERATURE CERAMICS FOR OXIDATION RESISTANCE II: THERMODYNAMIC MODELING OF THE HAFNIUM-TANTALUM-OXYGEN SYSTEM

Rahim Zaman, Elizabeth J. Opila, Bi-Cheng Zhou (Advisor)

University of Virginia, Department of Materials Science and Engineering, Charlottesville, VA

April 18, 2024

Abstract

Phase equilibria in the Hf-Ta-O system and HfO_2-Ta_2O_5 isoplethal section are modeled to optimize the thermal stability of HfC-TaC ceramics. Thermodynamic models under the CALculation of PHAse Diagrams (CALPHAD) framework are developed in conjunction with first-principles calculations and experimental data from the literature. Density functional theory (DFT) calculations of binary oxide thermodynamic properties agree with previous experimental data and predict cation disorder in $Hf_6Ta_2O_{17}$. Prior models of the Hf-Ta system, revised ones of the Hf-O system, and present ones of the Ta-O system are included in the ternary modeling. The ternary oxide series, $Hf_{(n-5)/2}Ta_2O_n$, is modeled as three solid solutions with disordered cation sublattices that increase in stability with structure size due to entropic stabilization. The current models predict that $Hf_4Ta_2O_{13}$ is metastable, consistent with lack of experimental evidence supporting its stability. The computed phase diagrams improve upon previous ones and predict that optimal thermal stability occurs at compositions between 3 HfC : 1 TaC and 4 HfC : 1 TaC.

1. Introduction

Ultra-high temperature ceramics (UHTCs) have the highest achievable melting temperatures above 3000 ^oC [1]. Due to the high thermal conductivity of UHTCs, they are considered potential materials for aerospace applications by the National Aeronautics and Space Administration (NASA) [2-4]. In particular, hafnium carbide (HfC) and tantalum carbide (TaC) are the UHTCs with the highest respective melting temperatures of 3900 ^oC and 3880 ^oC [5]. Nevertheless, HfC and TaC respectively oxidize to form HfO_2 and Ta_2O_5 with inadequate protective capability, and severe oxidation within minutes of oxygen exposure above 1600 ^oC limits the application of the carbides. HfC-TaC solution phases have been observed to form a densely packed, thermal-shock resistant, and adherent $Hf_6Ta_2O_{17}$ superstructure that is part of the $Hf_{(n-5)/2}Ta_2O_n$ homologous series [6], where $13 \leq n \leq 21$ [7]. $Hf_6Ta_2O_{17}$ has been found to have slower oxygen conduction compared to that of HfO_2 and Ta_2O_5 [8, 9], which is desirable for extreme condition applications including hypersonic aircraft design, thermal protection systems, and propulsion systems. However, the phase equilibria in the Hf-Ta-O system and HfO_2-Ta_2O_5 isoplethal section, including the stabilities of $Hf_{(n-5)/2}Ta_2O_n$ and $Hf_6Ta_2O_{17}$, remain unclear. The present study, described in more detail in an upcoming publication [10], is a continuation of [11] and models the phase equilibria in the ternary system using the CALculation of PHAse Diagrams (CALPHAD) method [12], incorporating the Ta-O models described in previous papers by the authors [11, 13]. The method combines calculated thermochemical properties with experimental data to determine optimized phase diagrams.

2. Review of Prior Experimental Data

2.1. Phases and Transformations in the Hf-Ta-O System.

The ambient pressure, equilibrium phases in the Hf-Ta-O system include hexagonal close-packed (HCP) α-Hf, body-centered cubic (BCC) β-Hf, BCC Ta, three HfO_2 polymorphs (monoclinic (M), tetragonal (T), and face-centered cubic (C)), two Ta_2O_5 polymorphs (orthorhombic (O) and tetragonal (T)), O-$Hf_{(n-5)/2}Ta_2O_n$, liquid, and gas [14]. While the stable O-Ta_2O_5 crystal structure is still debated, the β modification refined by Hummel et al. [15] is used for the present density functional theory (DFT) calculations and modeling due to its similarity to T-Ta_2O_5 [16], as the authors previously described in detail [11, 13]. The chosen β modification is nonstoichiometric with a

composition of $Ta_{24}O_{62}$ due to partial occupancy of oxygen sites. Crystal structures and phase transformations in the Hf-Ta-O system modeled in the current study are tabulated in the Part I paper [11].

2.2. Cation Disorder and Kinetic Metastability in O-$Hf_{(n-5)/2}Ta_2O_n$

Cation disorder in the O-$Hf_{(n-5)/2}Ta_2O_n$ series is very likely based on experimental evidence of it in isostructural O-$Zr_6Nb_2O_{17}$ [17], O-$Zr_{10}Nb_2O_{25}$ [18], O-$Zr_6Ta_2O_{17}$ [7], and O-$Hf_6Nb_2O_{17}$ [7]. Recent high temperature oxide melt solution calorimetry experiments of O-$A_6B_2O_{17}$, where A is Hf or Zr and B is Ta or Nb, by Voskanyan et al. [19] provide more direct evidence of cation disorder in O-$Hf_6Ta_2O_{17}$ and by extension, O-$Hf_{(n-5)/2}Ta_2O_n$. The study found that each ternary oxide has a positive enthalpy of formation from the respective binary oxides and requires considerable entropy to be stabilized. Since configurational entropy has a much higher magnitude than that of vibrational entropy in solid phases, Voskanyan et al. concluded that the former, arising from cation disorder, stabilizes the structures. Spurling et al. [20] further validated configurational cation disorder in O-$A_6B_2O_{17}$ structures using ex-situ and in-situ high temperature X-ray diffraction (XRD) of ternary and quinary O-$A_6B_2O_{17}$ phases. The ex-situ and in-situ experiments respectively resulted in O-$Hf_6Ta_2O_{17}$ stabilization temperatures of 1273 K and 1423 K, the difference of which with time indicating kinetic metastability. The longer timescale ex-situ value was used in the present study due to its improved accuracy for kinetically metastable O-$Hf_6Ta_2O_{17}$. The current CALPHAD models incorporate the cation disorder, as well as kinetic metastability, of O-$Hf_6Ta_2O_{17}$ and by extension, of O-$Hf_{(n-5)/2}Ta_2O_n$.

2.3. Prior Studies of the HfO_2-Ta_2O_5 Isoplethal Section

The first phase diagram of the HfO_2-Ta_2O_5 isoplethal section across the entire compositional range was constructed by Turcotte [21] using phase data from thermal arrest measurements, XRD, and electron microscopy. Turcotte concluded that the Ta_2O_5 phase acts as a solid solution or series of homologous structures based on similar XRD patterns between 3.9 and 9 mol% HfO_2. A comprehensive HfO_2-Ta_2O_5 isoplethal section was constructed by McCormack et al. [14] using thermal arrest measurements and in-situ X-ray powder diffraction (XRPD) with a conical nozzle levitator system to accurately measure the invariant transformation, solidus, and liquidus temperatures, equilibrium phases, and reversibility of phase transitions. The phase diagram was revised [22] to satisfy Hollman's Rule [23-25] and was used as the basis for the current CALPHAD models. Inconsistencies in the phase diagram, including lack of entropic stabilization and kinetic metastability and absence of an increase in stability with higher cation disorder [19] of the O-$Hf_{(n-5)/2}Ta_2O_n$ phase, were resolved by the present CALPHAD models.

3. Methods

3.1. First-Principles Calculations

As inputs for the CALPHAD models, 0-K and finite-temperature properties of M-HfO_2, O-Ta_2O_5, and O-$Hf_6Ta_2O_{17}$ were calculated using DFT and phonon calculations under the quasiharmonic approximation (QHA). The ordered form of O-$Hf_6Ta_2O_{17}$, although inconsistent with the 73-90 % cation disorder observed in the present mixing energies and prior experimental studies [19, 20], was used for the 0-K formation enthalpy and phonon calculations to reach manageable computational costs. Figure 1 shows the crystal structures of the oxides used for the first-principles calculations [7, 15, 26]. The DFT calculations run in the Vienna Ab initio Simulation Package (VASP) will be described in detail in an upcoming publication [10]. The local density approximation (LDA) functional [27] was used based on computations of the oxide formation enthalpies using five exchange-correlation functionals. Additional calculated properties include entropies (S), heat capacities (C_p), and Gibbs energies (G) of M-HfO_2 and O-$Hf_6Ta_2O_{17}$, and mixing enthalpies (ΔH_{mix}) of Ta and Hf in O-Ta_2O_5 and O-$Hf_6Ta_2O_{17}$. For validation, the heat capacities were compared to prior data from the literature. Phonon calculations were not performed on the O-Ta_2O_5 phase due to the overly high computational costs of modeling the oxygen partial occupancy in the chosen β modification [15].

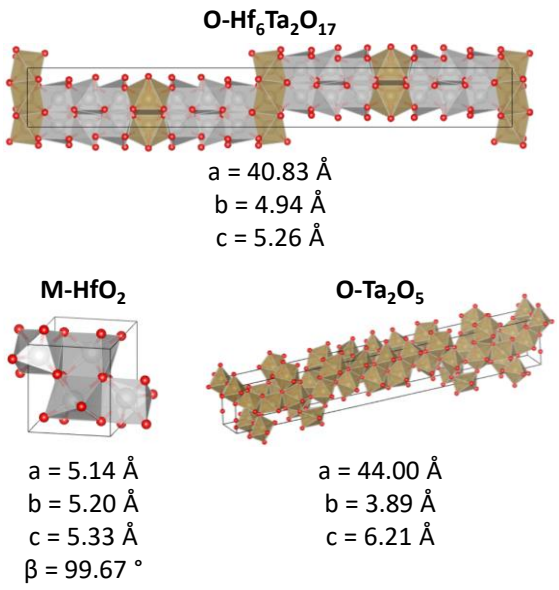

Figure 1. Crystal structures of O-$Hf_6Ta_2O_{17}$ [7], M-HfO_2 [26], and O-Ta_2O_5 [15] used for the current DFT computations.

0-K formation enthalpies of the oxides were calculated using Equations 1-3, where (E_0) is the total energy of the corresponding structure from full relaxation with DFT. The O_2 energy is that of an isolated molecule in a cubic 10 x 10 x 10 Å cell with spin polarization due to the unpaired electrons in its triplet ground state [28].

$$\Delta H_{f,0-K}^{O-Ta_2O_5} = E_0(Ta_2O_5) - 2E_0(Ta) - \frac{5}{2}E_0(O_2) \quad (1)$$

$$\Delta H_{f,0-K}^{M-HfO_2} = E_0(HfO_2) - E_0(Hf) - E_0(O_2) \quad (2)$$

$$\Delta H_{f,0-K}^{O-Hf_6Ta_2O_{17}} = E_0(Hf_6Ta_2O_{17}) - 6E_0(HfO_2) - E_0(Ta_2O_5) \quad (3)$$

To determine whether the error in the DFT formation enthalpies resulted from the choice of Ta_2O_5 structure, further values were calculated for O-$Hf_6Ta_2O_{17}$ and isostructural O-$Hf_6Nb_2O_{17}$ [7]. Total energies of the β (*C2mm*), T (*Pmm2*), B (*C2/c*), β (*Pccm*), δ (*P6/mmm*), β (*Pmma*), λ (*Pbam*), *Pmmn*, and γ (*I4₁/amd*) Ta_2O_5 modifications described in the Part I paper [11], and the P (*I4₁/amd*) [29, 30], R (*A2/m*) [31], N (*C2/m*) [32], M (*I4/mmm*) [33], and B (*C2/c*) [34] Nb_2O_5 modifications were input into Equation 3 for the respective formation enthalpy calculations.

Phonon dispersions and vibrational entropies were computed in Phonopy [35] under the harmonic approximation. Heat capacities and Gibbs energies as functions of temperature were calculated in Phonopy using the third-order Birch-Murnaghan [36] equation of state and quasiharmonic approximation (QHA). ΔG and ΔS were used to compute the 298-K enthalpies of formation using Equation 4 [37], in which F is the Helmholtz free energy, E_0 is the enthalpy at 0 K, and F_{vib} is the vibrational free energy contribution.

$$F(V,T) = E_0(V) + F_{vib}(V,T) \quad (4)$$

Dilute enthalpies of mixing of Ta and Hf in O-Ta_2O_5 were computed by DFT calculations of the $Hf_{23}Ta_1O_{62}$ ($x_{Hf_2O_5}$ = 0.96, $x_{Ta_2O_5}$ = 0.04) and $Hf_1Ta_{23}O_{62}$ ($x_{Hf_2O_5}$ = 0.04, $x_{Ta_2O_5}$ = 0.96) structures, and those of the $Hf_{24}O_{62}$ and $Ta_{24}O_{62}$ reference ones, as shown in Equations 5 and 6, respectively.

$$\Delta H_{mix,dilute}^{Hf_{23}Ta_1O_{62}} = E_0(Hf_{23}Ta_1O_{62}) - \frac{23}{24}E_0(Hf_{24}O_{62}) - \frac{1}{24}E_0(Ta_{24}O_{62}) \quad (5)$$

$$\Delta H_{mix,dilute}^{Hf_1Ta_{23}O_{62}} = E_0(Hf_1Ta_{23}O_{62}) - \frac{23}{24}E_0(Ta_{24}O_{62}) - \frac{1}{24}E_0(Hf_{24}O_{62}) \quad (6)$$

Enthalpies of mixing of Ta and Hf in O-$Hf_6Ta_2O_{17}$ between the compositions Hf_8O_{17} and Ta_8O_{17} were calculated using special quasirandom structures (SQS) created using the Alloy Theoretic Automated Toolkit (ATAT) [38]. Equation 7, in which n is an integer from 1 to 3, was used to compute the mixing enthalpies. Mechanical instabilities in the SQS were accounted for using the inflection-detection method [39].

$$\Delta H_{mix}^{Hf_{8n}Ta_{32-8n}O_{68}} = E_0(Hf_{8n}Ta_{32-8n}O_{68}) - nE_0(Hf_8O_{17}) - (4-n)E_0(Ta_8O_{17}) \quad (7)$$

3.2. Thermodynamic Models

All phases in the Hf-Ta-O system were modeled using the compound energy formalism (CEF), the details of which are described in the Part I paper [11]. Due to the stoichiometry of the Ta_2O_5 and O-$Hf_{(n-5)/2}Ta_2O_n$ phases [13, 22], their vacancy concentrations and binary excess interaction terms

with vacancies, were considered negligible. Binary interaction parameters $\left({}^{v}L_{ij}\right)$ with a linear temperature dependence were added as needed to fit the experimental phase data. Gibbs energy equation parameters were optimized in the Thermo-Calc software [40]. Parameters from the Scientific Group Thermodata Europe (SGTE) database [41] were used for the elemental reference states.

Modeled phases include those in the binary Hf-O, Hf-Ta, and Ta-O systems, as well as O- and T-Ta_2O_5 solid solutions, $Hf_4Ta_2O_{13}$, $Hf_6Ta_2O_{17}$, $Hf_8Ta_2O_{21}$, and a liquid phase. Existing CALPHAD models of the Hf-O system by Wang [42] were modified to correct errors and more closely estimate the maximum oxygen deficiency in the C-HfO_2 phase, which was previously determined to be 64 at%, by metallographic and chemical analyses [43-45]. Models of the Hf-Ta and Ta-O systems were respectively adopted from those of Guillermet [46] and those published by the authors [11, 13]. The homologous series of O-Ta_2O_5 and T-Ta_2O_5 [21, 22] were modeled as ionic solutions with the sublattice model $(Hf^{+4},Ta^{+5})_2(O^{-2},Va)_5$. Gibbs energy parameters of both phases were optimized to fit experimental phase data [14, 20, 21]. The $Hf_{(n-5)/2}Ta_2O_n$ homologous series [6, 14] was modeled as three solid solutions with kinetic metastability and cation disorder [7, 19, 20] using the sublattice models $(Hf^{+4},Ta^{+5})_6(O^{-2},Va)_{13}$, $(Hf^{+4},Ta^{+5})_8(O^{-2},Va)_{17}$, and $(Hf^{+4},Ta^{+5})_{10}(O^{-2},Va)_{21}$ to respectively describe O-$Hf_4Ta_2O_{13}$, O-$Hf_6Ta_2O_{17}$, and O-$Hf_8Ta_2O_{21}$. The Gibbs energy parameters of O-$Hf_6Ta_2O_{17}$ were obtained by fitting the SQS mixing enthalpies and from the experimental phase data [14, 20]. Those of O-$Hf_4Ta_2O_{13}$ and O-$Hf_8Ta_2O_{21}$ were qualitatively adjusted to result in an increase in stability of $Hf_{(n-5)/2}Ta_2O_n$ with larger structure size to reflect cation entropy stabilization [19]. The liquid phase was modeled by the ionic two-sublattice model developed by Hillert et al. [47], as: $(Hf^{+4},Ta^{+5})_{2y_{O^{-2}}+Qy_{Va^{-Q}}}(O^{-2},Va^{-Q})_{4y_{Hf^{+4}}+5y_{Ta^{+5}}}$, where $Q = 4y_{Hf^{+4}} + 5y_{Ta^{+5}}$. Gibbs energy parameters were fit to experimental phase data from McCormack et al. [14] and Turcotte [21]. The optimized thermodynamic models of the Hf-Ta-O system will be included in an upcoming publication [10].

4. Results and Discussion

The 298-K DFT formation enthalpy of M-HfO_2 (-1162.93 kJ/mol) using the LDA functional results in a -4.24 % difference from the experimental value in the SGTE database [48] and the 0-K value of the T modification of O-Ta_2O_5 (-2047.38 kJ/mol) results in a +0.08 % difference. Despite the high accuracy for the binary oxides, the calculated 0-K values for both O-$Hf_6Ta_2O_{17}$ and O-$Hf_6Nb_2O_{17}$ shown in Table 1 are all negative and significantly differ from the positive values from oxide melt solution calorimetry [19], indicating that the error is not from the choice of Ta or Nb oxide modification. Rather, the error can be attributed to that from the LDA functional as will be shown by the mixing enthalpy results.

Table 1. 0-K DFT formation enthalpies of O-$Hf_6Ta_2O_{17}$ and O-$Hf_6Nb_2O_{17}$ from M-HfO_2 [26] and Ta_2O_5 and Nb_2O_5 modifications with available structural data compared to oxide melt solution calorimetric values of 42.94 ± 7.03 kJ/mol and 38.44 ± 6.75 kJ/mol, respectively [19].

Ta_2O_5 or Nb_2O_5 Modification	Calculated 0-K ΔH_f (kJ/mol)	Difference from Experimental (%)
O-$Hf_6Ta_2O_{17}$		
B (*C2/c*)	-13.20	-130.75
γ (*I4₁/amd*)	-18.66	-143.44
λ (*Pbam*)	-24.93	-158.05
β (*Pmma*)	-25.52	-159.44
Pmmn	-28.00	-165.20
β (*C2mm*)	-74.29	-273.01
T (*Pmm2*)	-138.83	-423.32
δ (*P6/mmm*)	-198.84	-563.07
β (*Pccm*)	-246.36	-673.73
O-$Hf_6Nb_2O_{17}$		
B (ζ) (*C2/c*)	-15.82	-141.16
P (η) (*I4₁/amd*)	-28.01	-172.88
N (*C2/m*)	-29.16	-175.87
R (*A2/m*)	-31.62	-182.26
M (*I4/mmm*)	-37.98	-198.80

The calculated heat capacity of M-HfO_2 under the QHA as a function of temperature is shown in Figure 2 and agrees with that in the SGTE database [48], that calculated using the stoichiometric Hf-O CALPHAD model [42], and

that from prior ab-initio molecular dynamics (AIMD) and QHA calculations [49]. Figure 3 shows the heat capacity of O-$Hf_6Ta_2O_{17}$ calculated under the QHA, which agrees with the current thermodynamic models, as well as with values measured by Li et al. [50] using the comparison method with laser flash analysis. The aforementioned values underestimate those of Perepezko [51], which were obtained using the comparison method with laser flash analysis. The values of Perepezko [51] are expected to be less accurate, as they indicate a sharp rise in heat capacity of a densely packed structure.

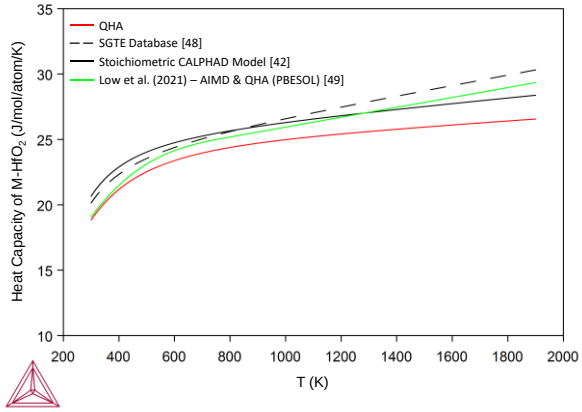

Figure 2. Constant pressure heat capacities of M-HfO_2 as a function of temperature calculated by the QHA compared to prior AIMD and QHA calculations [49], a stoichiometric CALPHAD model [42], and experimental values from the SGTE database [48].

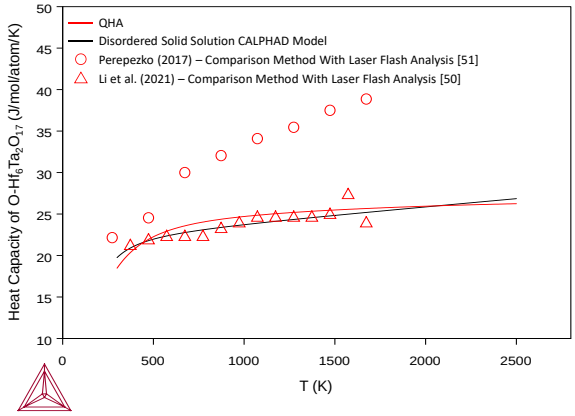

Figure 3. Constant pressure heat capacities of O-$Hf_6Ta_2O_{17}$ as a function of temperature calculated by the QHA compared to those from the present CALPHAD model and experimental measurements by Li et al. [50] and Perepezko [51].

Mixing enthalpies of Ta and Hf in the O-Ta_2O_5 solid solution fitted to phase data of the HfO_2-Ta_2O_5 system under the current model parameters are shown in Figure 4. SQS mixing enthalpies of Ta and Hf in O-$Hf_6Ta_2O_{17}$ fitted to a zero- and first-order interaction parameter Redlich-Kister polynomial [52] are shown in Figure 5. Based on the minimum mixing energy at 75 at% Hf, the calorimetric formation enthalpy of 42.94 $\pm$ 7.03 kJ/mol [19], and a cationic configurational entropy of 28.05 J/mol/K, a minimum stabilization temperature of 1531 $\pm$ 251 K is predicted for O-$Hf_6Ta_2O_{17}$, consistent with the 1273 K value measured by Spurling et al. [20]. The SQS mixing enthalpies, like the formation enthalpies, of O-$Hf_6Ta_2O_{17}$ are negative in contrast to prior calorimetric findings [19]. Calculated 0-K formation enthalpies of the 75 % cation disorder SQS structure using each modification of O-Ta_2O_5 are more negative and have a larger error relative to the positive calorimetric formation enthalpy [19] than that of the ordered structure. This indicates that the DFT error in the signs of the O-$Hf_6Ta_2O_{17}$ formation and mixing enthalpies is due to underestimation of the total energies by the LDA functional rather than the choice of O-Ta_2O_5 modification or use of ordered ternary oxide structure for the former.

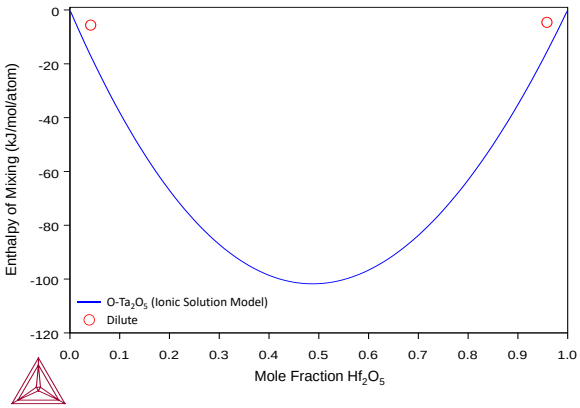

Figure 4. Fit of mixing enthalpies of Hf and Ta in the O-Ta_2O_5 solid solution as a function of Hf content using the ionic solution model based on experimental HfO_2-Ta_2O_5 isoplethal section phase data [14]. Dilute mixing enthalpies from DFT calculations are also shown.

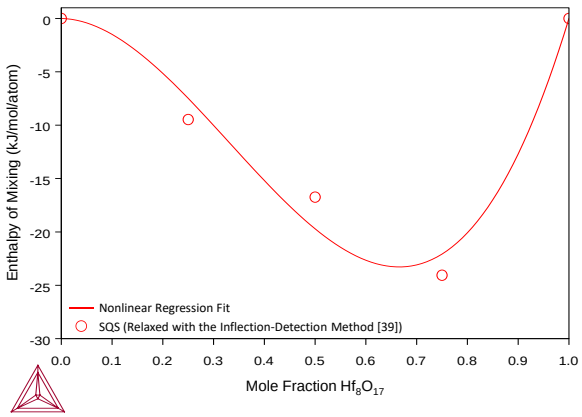

Figure 5. Fit of SQS mixing enthalpies of Hf and Ta in O-$Hf_6Ta_2O_{17}$ as a function of Hf content using nonlinear regression.

The revised Hf-O phase diagram (Figure 6) agrees with experimental phase data in the literature [43-45, 53]. Hf-Ta-O models optimized using zero- and first-order binary interaction parameters sufficiently describe the experimental HfO_2-Ta_2O_5 isoplethal section and will be tabulated in an upcoming publication [10]. A calculated isothermal section of the Hf-Ta-O system at 1773 K is displayed in Figure 7 and better agrees with experimental phase data [14] relative to previous ones [54, 55].

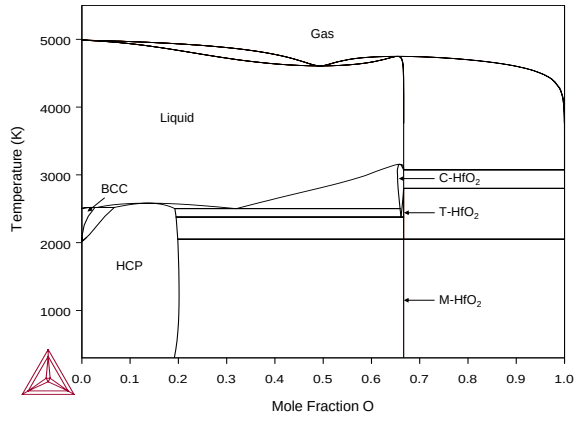

Figure 6. Revised Hf-O phase diagram.

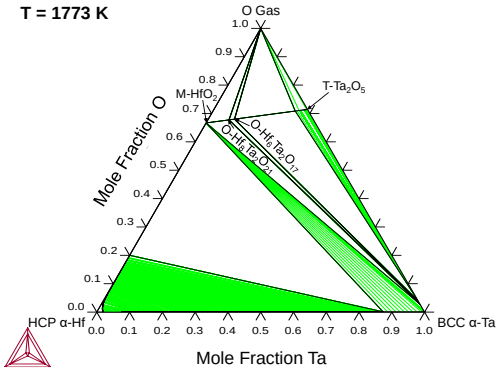

Figure 7. Calculated isothermal Hf-Ta-O section at 1773 K.

The calculated HfO_2-Ta_2O_5 isoplethal section between 273 and 3500 K (Figure 8) agrees well with experimental phase data from Spurling et al. [20] and Turcotte [21] but differs from the isoplethal section by McCormack et al. [22]. The phase transitions and invariant equilibria of the latter are compared to current results in Figure 8. Primary differences are those in the stabilities of the O-$Hf_{(n-5)/2}Ta_2O_n$ phases and those in the Ta_2O_5-rich liquidus. In contrast to the phase diagram of McCormack et al., the current study finds that O-$Hf_4Ta_2O_{13}$, O-$Hf_6Ta_2O_{17}$, and O-$Hf_8Ta_2O_{21}$ respectively increase in stability due to increasing entropic stabilization and have minimum stabilization temperatures above 298 K due to kinetic metastability. This finding is consistent with more recent experimental ones by Spurling et al. [20] and Voskanyan et al. [19]. In the present study, $Hf_4Ta_2O_{13}$ requires the highest enthalpy of formation and most negative entropy of formation of the ternary oxides for it to be stable, unlike the expected trends $\Delta H_f^{O-Hf_4Ta_2O_{13}} < \Delta H_f^{O-Hf_6Ta_2O_{17}} < \Delta H_f^{O-Hf_8Ta_2O_{21}}$ and $(most\ negative)\ S_{conf}^{Hf_8Ta_2O_{21}} < S_{conf}^{Hf_6Ta_2O_{17}} < S_{conf}^{Hf_4Ta_2O_{13}}$. Due to these discrepancies, as well as lack of data supporting the stability of $A_4B_2O_{13}$ (where A is Hf or Zr and B is Ta or Nb) and the prior concluded metastability of $Hf_3Ta_2O_{11}$ [56], $Hf_4Ta_2O_{13}$ is also concluded to be metastable. Regarding the differences in the Ta_2O_5-rich liquidus, the current models overestimate the T-Ta_2O_5 liquidus relative to that of McCormack et al. In addition, they do not consider a monotectic or miscibility gap due to lack of confirmation of its existence by X-ray scattering data [14], and instead predict a congruent melting point at x_{HfO2} = 0.145 and T = 2236 K.

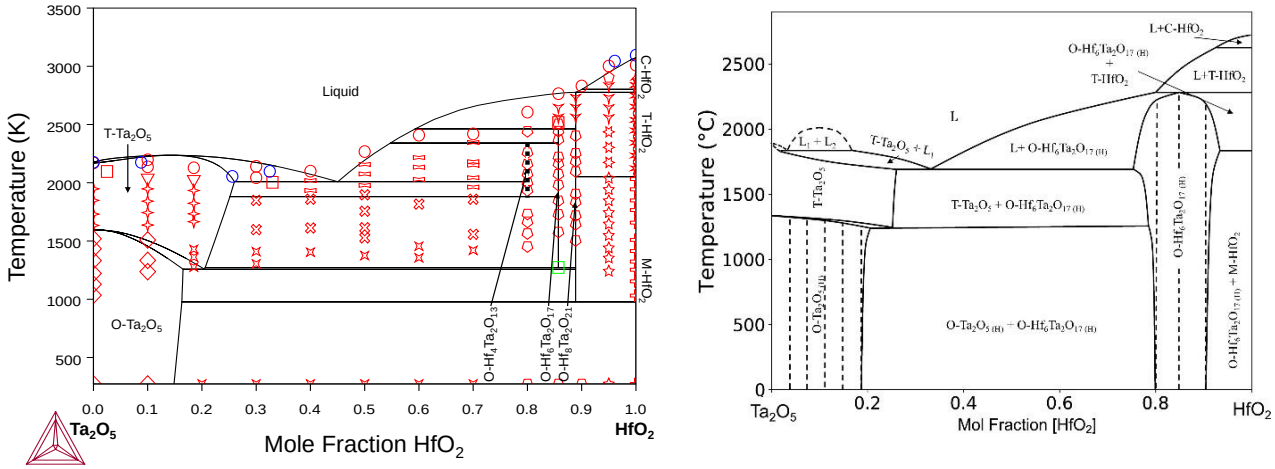

Figure 8. (Left) Calculated HfO_2-Ta_2O_5 isoplethal section. Experimental data from [20] (Green), [14] (Red), and [21] (Blue). The dotted phase boundary of $Hf_4Ta_2O_{13}$ in the calculated isoplethal section indicates metastability. (Right) Experimental HfO_2-Ta_2O_5 isoplethal section constructed and revised by McCormack et al. [14, 22]. Dashed lines specify regions for which additional experiments are needed for validation. Figure from S. J. McCormack et al., "Reply to comments: "In-situ determination of the HfO_2-Ta_2O_5-temperature phase diagram up to 3000°C"," *J. Am. Ceram. Soc.*, vol. 102, no. 11, 2019 republished with permission from Elsevier; Permission was conveyed through Copyright Clearance Center, Inc.

5. Conclusions

Thermodynamic properties of M-HfO_2 and O-Ta_2O_5 are accurately described by DFT calculations and support cation disorder in the O-$Hf_{(n-5)/2}Ta_2O_n$ phase in agreement with prior experimental findings. The modified phase diagram of the Hf-O system and new ones of the Hf-Ta-O system agree with experimental phase data, and the latter show that the O-$Hf_{(n-5)/2}Ta_2O_n$ phase increases in stability with higher HfO_2 content and has minimum stabilization temperatures above 298 K. These phenomena occur due to cation entropy stabilization and kinetic metastability, respectively. Consequently, HfC-TaC UHTCs with compositions between 3 HfC : 1 TaC and 4 HfC : 1 TaC are predicted to have the optimal thermal stability. Further studies pertaining to the thermodynamics and kinetics of oxidation are required to compare oxygen transport in the O-$Hf_{(n-5)/2}Ta_2O_n$ phase to those of HfO_2 and Ta_2O_5 and are currently being carried out by the authors.

Declaration of Competing Interest

The authors declare that they have no known competing financial interests or personal relationships that could have appeared to influence the work reported in this paper.

Acknowledgements

R.Z. acknowledges support from the Virginia Space Grant Consortium (VSGC) Graduate Research Fellowship and University of Virginia Engineering Distinguished Fellowship. B.-C.Z. acknowledges support from the University of Virginia start-up funds. All authors acknowledge support from the Office of Naval Research (ONR) through Grant No. N00014-19-1-2274 by the U.S. Department of Defense under program managers Dr. Eric Wuchina and Dr. Eric Marineau. The authors acknowledge Research Computing at the University of Virginia for providing computational resources and technical support that have contributed to the results reported within this publication. URL: https://re.virginia.edu.

References

[1] W. G. Fahrenholtz and G. E. Hilmas "Ultra-high temperature ceramics: Materials for extreme environments," *Scripta Mater.*, vol. 129, pp. 94-99, 2017.

[2] J. W. Dankanich and R. L. Frederick, "Marshall Space Flight Center: Research and Technology Report 2020," National Aeronautics and Space Administration, 2020, pp. 64-65.

[3] C. Robinson, "Overview of Environmental Durability Coatings and Test Capabilities," Hypersonic Propulsion Materials and Structures Workshop. National Aeronautics and Space Administration, 2019.

[4] S. M. Johnson, "Ultra High Temperature Ceramics," National Aeronautics and Space Administration, 2015.

[5] W. G. Fahrenholtz, "Refractory Diborides of Zirconium and Hafnium," *J. Am. Ceram. Soc.*, vol. 90, no. 5, pp. 1347-1364, 2007.

[6] F. M. Spiridonov, M. N. Mulenkova, V. I. Tsirel'nikov, and L. N. Komissarova, "Intermediate Phases in the HfO_2-Ta_2O_5 System," *Russ. J. Inorg. Chem.*, vol. 26, no. 6, pp. 922-923, 1981.

[7] S. J. McCormack and W. M. Kriven, "Crystal structure solution for the $A_6B_2O_{17}$ (A = Zr, Hf; B = Nb, Ta) superstructure," *Acta Crystallogr. B*, vol. 75, no. 2, pp. 227-234, 2019.

[8] J. Zhang, S. Wang, W. Li, Y. Yu, and J. Jiang, "Understanding the oxidation behavior of Ta–Hf–C ternary ceramics at high temperature," *Corros. Sci.*, vol. 164, 108348, 2020.

[9] C. Zhang, B. Boesl, and A. Agarwal, "Oxidation resistance of tantalum carbide-hafnium carbide solid solutions under the extreme conditions of a plasma jet," *Ceram. Int.*, vol. 43, no. 17, pp. 14798-14806, 2017.

[10] R. Zaman, E. J. Opila, and B.-C. Zhou, "Thermodynamic Modeling of the Hf-Ta-O System for the Design of Oxidation Resistant HfC-TaC Ceramics," Under Review.

[11] R. Zaman and B.-C. Zhou, "Design of Ultra-High Temperature Ceramics for Oxidation Resistance," in Virginia Space Grant Consortium Student Research Conference, Newport News, VA, 2023.

[12] N. Saunders and A. P. Miodownik, *CALPHAD (Calculation of Phase Diagrams): A Comprehensive Guide*, 1 ed.: Pergamon, 1998.

[13] K. J. Meisner, R. Zaman, and B.-C. Zhou, "Thermodynamic modeling of the Ta-O system," *Calphad*, vol. 76, 102391, 2022.

[14] S. J. McCormack, K.-P. Tseng, R. J. K. Weber, D. Kapush, S. V. Ushakov, A. Navrotsky, and W. M. Kriven, "In-situ determination of the HfO_2–Ta_2O_5-temperature phase diagram up to 3000°C," *J. Am. Ceram. Soc.*, vol. 102, no. 8, pp. 4848-4861, 2018.

[15] H.-U. Hummel, R. Fackler, and P. Remmert, "Tantaloxide durch Gasphasenhydrolyse, Druckhydrolyse und Transportreaktion aus 2H-TaS_2: Synthesen von TT-Ta_2O_5 und T-Ta_2O_5 und Kristallstruktur von T-Ta_2O_5 (in German)," *Chem. Ber.*, vol. 125, pp. 551-556, 1992.

[16] X. Q. Liu, X. D. Han, Z. Zhang, L. F. Ji, and Y. J. Jiang, "The crystal structure of high temperature phase Ta_2O_5," *Acta Mater.*, vol. 55, no. 7, pp. 2385-2396, 2007.

[17] S. Schmid, J. G. Thompson, R. L. Withers, V. Petříček, N. Ishizawa, and S. Kishimoto, "Re-Refinement of Composite Modulated $Nb_2Zr_{x-2}O_{2x+1}$ (x = 8) Using Synchrotron Radiation Data," *Acta Crystallogr. B*, vol. 53, no. 6, pp. 851-860, 1997.

[18] K. Fütterer, S. Schmid, J. G. Thompson, R. L. Withers, N. Ishizawa, and S. Kishimoto, "The Structure Refinement of Compositely Modulated $Nb_2Zr_{x-2}O_{2x+1}$ (x = 12)," *Acta Crystallogr. B*, vol. 51, no. 5, pp. 688-697, 1995.

[19] A. A. Voskanyan, K. Lilova, S. J. McCormack, W. M. Kriven, and A. Navrotsky, "A new class of entropy stabilized oxides: Commensurately modulated $A_6B_2O_{17}$ (A = Zr, Hf; B = Nb, Ta) structures," *Scripta Mater.*, vol. 204, 114139, 2021.

[20] R. J. Spurling, C. Skidmore, N. S. McIlwaine, and J.-P. Maria, "Phase equilibria and metastability in the high-entropy $A_6B_2O_{17}$ oxide

family with A = Zr, Hf and B = Nb, Ta," *J. Mater. Sci.*, vol. 58, no. 14, pp. 6164-6173, 2023.

[21] R. P. Turcotte, *Phase Relationships in High Temperature Ceramics*, Naval Surface Weapons Center, Silver Spring, Maryland, 1987.

[22] S. J. McCormack, K.-P. Tseng, R. J. K. Weber, D. Kapush, S. V. Ushakov, A. Navrotsky, and W. M. Kriven, "Reply to comments: "In-situ determination of the HfO_2-Ta_2O_5-temperature phase diagram up to 3000°C"," *J. Am. Ceram. Soc.*, vol. 102, no. 11, pp. 7028-7030, 2019.

[23] P. P. Fedorov, "Comment on the paper: Scott J. McCormack, Kuo-Pin Tseng, Richard Weber et al "In situ determination of the HfO_2–Ta_2O_5-temperature phase diagram up to 3000°C"," *J. Am. Ceram. Soc.*, vol. 102, no. 11, pp. 7026-7027, 2019.

[24] V. N. Vigdorovich and A. N. Krestovnikov, "Relative Position of Phase Equilibrium Curves for Two-Component Systems," *Russ. J. Phys. Chem.*, vol. 34, no. 9, pp. 946-949, 1960.

[25] H. Lipson and A. J. C. Wilson, "Some Properties of Alloy Equilibrium Diagrams Derived from the Principle of Lowest Free Energy," *J. Iron Steel I.*, vol. 142, no. 2, pp. 107-118, 1940.

[26] A. Jain, S. P. Ong, G. Hautier, W. Chen, W. D. Richards, S. Dacek, S. Cholia, D. Gunter, D. Skinner, G. Ceder, and K. A. Persson, "Commentary: The Materials Project: A materials genome approach to accelerating materials innovation," *APL Mater.*, vol. 1, no. 1, 011002, 2013.

[27] D. M. Ceperley and B. J. Alder, "Ground State of the Electron Gas by a Stochastic Method," *Phys. Rev. Lett.*, vol. 45, no. 7, pp. 566-569, 1980.

[28] O. Khabashesku and B. Ellis, *Singlet Oxygen Oxidized Materials and Methods of Making and Using Same*, United States, 2009.

[29] J.-H. Yuan, K.-H. Xue, Q. Chen, L. R. C. Fonseca, and X.-S. Miao, "Ab Initio Simulation of Ta_2O_5: A High Symmetry Ground State Phase with Application to Interface Calculation," *Ann. Phys. (Berlin)*, vol. 531, no. 8, 1800524, 2019.

[30] F. Laves, R. Moser, and W. Petter, "Eine mit α-Ta_2O_5 verwandte Nb_2O_5-Modifikation: η-Nb_2O_5 (In German)," *Naturwissenschaften*, vol. 52, no. 22, pp. 617-618, 1965.

[31] R. Gruehn, "Eine weitere neue Modifikation des niobpentoxids (In German)," *J. Less-Common Met.*, vol. 11, no. 2, pp. 119-126, 1966.

[32] S. Andersson, "The Crystal Structure of N-Nb_2O_5, Prepared in the Presence of Small Amounts of LiF," *Z. Anorg. Allg. Chem.*, vol. 351, no. 1-2, pp. 106-112, 1967.

[33] W. Mertin, S. Andersson, and R. Gruehn, "Über die Kristallstruktur von M-Nb_2O_5 (In German)," *J. Solid State Chem.*, vol. 1, no. 3-4, pp. 419-424, 1970.

[34] T. S. Ercit, "Refinement of the Structure of ζ-Nb_2O_5 and Its Relationship to the Rutile and Thoreaulite Structures," *Miner. Petrol.*, vol. 43, no. 3, pp. 217-223, 1991.

[35] A. Togo and I. Tanaka, "First principles phonon calculations in materials science," *Scripta Mater.*, vol. 108, pp. 1-5, 2015.

[36] F. Birch, "Finite Elastic Strain of Cubic Crystals," *Phys. Rev.*, vol. 71, no. 11, pp. 809-824, 1947.

[37] S.-L. Shang, Y. Wang, and Z.-K. Liu, "Thermodynamic fluctuations between magnetic states from first-principles phonon calculations: The case of bcc Fe," *Phys. Rev. B*, vol. 82, no. 1, 014425, 2010.

[38] A. van de Walle, P. Tiwary, M. de Jong, D. L. Olmsted, M. Asta, A. Dick, D. Shin, Y. Wang, L.-Q. Chen, and Z.-K. Liu, "Efficient stochastic generation of special quasirandom structures," *Calphad*, vol. 42, pp. 13-18, 2013.

[39] A. van de Walle, Q. Hong, S. Kadkhodaei, and R. Sun, "The free energy of mechanically unstable phases," *Nat. Commun.*, vol. 6, 7559, 2015.

[40] J.-O. Andersson, T. Helander, L. Höglund, P. Shi, and B. Sundman, "Thermo-Calc & DICTRA, computational tools for materials science," *Calphad*, vol. 26, no. 2, pp. 273-312, 2002.

[41] A. T. Dinsdale, “SGTE data for pure elements,” *Calphad,* vol. 15, no. 4, pp. 317-425, 1991.

[42] C. Wang, “Experimental and Computational Phase Studies of the ZrO_2-based Systems for Thermal Barrier Coatings,” Department of Chemistry, Max-Planck-Institut für Metallforschung, Stuttgart, 2006.

[43] R. Ruh and V. A. Patel, “Proposed Phase Relations in the HfO_2-Rich Portion of the System Hf-HfO_2,” *J. Am. Ceram. Soc.,* vol. 56, no. 11, pp. 606-607, 1973.

[44] R. F. Domagala and R. Ruh, “The Hafnium-Oxygen System,” *T. Am. Soc. Metal.,* vol. 58, no. 2, pp. 164-175, 1965.

[45] E. Rudy and P. Stecher, “Zum Aufbau des Systems Hafnium-Sauerstoff (In German),” *J. Less-Common Met.,* vol. 5, no. 1, pp. 78-89, 1963.

[46] A. F. Guillermet, “Gibbs Energy Modelling of the Phase Diagram and Thermochemical Properties in the Hf-Ta System,” *Z. Metallkd.,* vol. 86, no. 6, pp. 382-387, 1995.

[47] M. Hillert, B. Jansson, B. Sundman, and J. Ågren, “A Two-Sublattice Model for Molten Solutions with Different Tendency for Ionization,” *Metall. Trans. A,* vol. 16A, pp. 261-266, 1985.

[48] Scientific Group Thermodata Europe, "SGTE Substance Database Version 6.0."

[49] J. J. Low, N. H. Paulson, M. D’Mello, and M. Stan, “Thermodynamics of monoclinic and tetragonal hafnium dioxide (HfO_2) at ambient pressure,” *Calphad,* vol. 72, 102210, 2021.

[50] H. Li, Y. Yu, S. Wang, P. Xiao, and T. Hu, “Low thermal conductivity $Hf_6Ta_2O_{17}$ ceramics fabricated by solvothermal and pressure-less sintering,” *Ceram. Int.,* vol. 47, no. 12, pp. 17711-17718, 2021.

[51] J. H. Perepezko, *New Oxide Materials for an Ultra High Temperature Environment*, University of Wisconsin, Madison, Wisconsin, 2017.

[52] O. Redlich and A. T. Kister, “Algebraic Representation of Thermodynamic Properties and the Classification of Solutions,” *Ind. Eng. Chem.,* vol. 40, no. 2, pp. 345-348, 1948.

[53] R. Ruh, H. J. Garrett, R. F. Domagala, and N. M. Tallan, “The System Zirconia-Hafnia,” *J. Am. Ceram. Soc.,* vol. 51, no. 1, pp. 23-27, 1968.

[54] Y. Yang, J. H. Perepezko, and C. Zhang, “Oxidation synthesis of $Hf_6Ta_2O_{17}$ superstructures,” *Mater. Chem. Phys.,* vol. 197, pp. 154-162, 2017.

[55] I. Tyshchenko and K. Korniyenko, *Hf-O-Ta Ternary Phase Diagram Evaluation*, MSI Eureka Stuttgart, Germany, vol. 74, 2017.

[56] D. Wiedemann, S. Orthmann, M. J. Mühlbauer, and M. Lerch, “Commensurate $Nb_2Zr_5O_{15}$: Accessible Within the Field $Nb_2Zr_xO_{2x+5}$ After All,” *ChemistryOpen,* vol. 8, no. 4, pp. 447-450, 2019.